論文 / 著書情報
Article / Book Information

Title	Band alignment of semiconductors and insulators using dielectric-dependent hybrid functionals: Toward high-throughput evaluation
Authors	Yoyo Hinuma, Yu Kumagai, Isao Tanaka, Fumiyasu Oba
Citation	Physical Review B, vol. 95, , pp. 075302-1-10
Pub. date	2017, 2
Copyright	(c) 2017 American Physical Society
DOI	http://dx.doi.org/10.1103/PhysRevB.95.075302

Band alignment of semiconductors and insulators using dielectric-dependent hybrid functionals: Toward high-throughput evaluation

Yoyo Hinuma,[1,2] Yu Kumagai,[3,4,*] Isao Tanaka,[1,2] and Fumiyasu Oba[2,3,5,†]

[1]*Department of Materials Science and Engineering, Kyoto University, Yoshida-Honmachi, Sakyo-ku, Kyoto 606-8501, Japan*

[2]*Center for Materials Research by Information Integration, National Institute for Materials Science, 1-2-1 Sengen, Tsukuba 305-0047, Japan*

[3]*Materials Research Center for Element Strategy, Tokyo Institute of Technology, 4259 Nagatsuta, Midori-ku, Yokohama 226-8503, Japan*

[4]*PRESTO, Japan Science and Technology Agency, 4-1-8 Honcho, Kawaguchi 332-0012, Japan*

[5]*Laboratory for Materials and Structures, Institute of Innovative Research, Tokyo Institute of Technology, 4259 Nagatsuta, Midori-ku, Yokohama 226-8503, Japan*

(Received 17 December 2016; published 3 February 2017)

The band alignment of prototypical semiconductors and insulators is investigated using first-principles calculations. A dielectric-dependent hybrid functional, where the nonlocal Fock exchange mixing is set at the reciprocal of the static electronic dielectric constant and the exchange correlation is otherwise treated as in the Perdew-Burke-Ernzerhof (PBE0) hybrid functional, is used as well as the Heyd-Scuseria-Ernzerhof (HSE06) hybrid and PBE semilocal functionals. In addition, these hybrid functionals are applied non-self-consistently to accelerate calculations. The systems considered include C and Si in the diamond structure, BN, AlP, AlAs, AlSb, GaP, GaAs, InP, ZnS, ZnSe, ZnTe, CdS, CdSe, and CdTe in the zinc-blende structure, MgO in the rocksalt structure, and GaN and ZnO in the wurtzite structure. Surface band positions with respect to the vacuum level, i.e., ionization potentials and electron affinities, and band offsets at selected zinc-blende heterointerfaces are evaluated as well as band gaps. The non-self-consistent approach speeds up hybrid functional calculations by an order of magnitude, while it is shown using HSE06 that the resultant band gaps and surface band positions are similar to the self-consistent results. The dielectric-dependent hybrid functional improves the band gaps and surface band positions of wide-gap systems over HSE06. The interfacial band offsets are predicted with a similar degree of precision. Overall, the performance of the dielectric-dependent hybrid functional is comparable to the GW_0 approximation based on many-body perturbation theory in the prediction of band gaps and alignments for most systems. The present results demonstrate that the dielectric-dependent hybrid functional, particularly when applied non-self-consistently, is promising for applications to systematic calculations or high-throughput screening that demand both computational efficiency and sufficient accuracy.

DOI: 10.1103/PhysRevB.95.075302

I. INTRODUCTION

The band alignment, also denoted as band lineup, is fundamentally and technologically important in the design and development of electronic devices, photovoltaics, photocatalysts, and so forth, which utilize the surfaces or heterointerfaces of semiconductors and insulators [1–7]. The surface band alignment provides the information of the valence band maximum (VBM) and conduction band minimum (CBM) with respect to the vacuum level, which are the negatives of the ionization potential (IP) and electron affinity (EA), respectively. These quantities involve surface dipole contributions, and therefore, the band positions are dependent on the surface orientation, composition, atomistic and electronic structure, and adsorption or contamination, all of which affect the surface dipole [3,8]. Similarly, the interfacial band alignment, which is determined by the valence and conduction band offsets at heterointerfaces, includes interfacial dipole contributions [1,2], although their effects tend to be smaller than those of the surface dipoles due to the formation of chemical bonding at the interfaces. Thus, the band alignment should be discussed after specifying the characters of the surfaces and interfaces.

Computational efficiency and accuracy are both needed for constructing band alignment theoretically as it requires systematic evaluations of IPs and EAs at surfaces or valence and conduction band offsets at heterointerfaces. A combination of bulk and surface or interface calculations is typically used to reduce computational costs, where only bulk systems are treated at a high level of approximation and they are electrostatically aligned with surfaces or interfaces treated using standard local or semilocal density functionals [9–11]. This approach is based on the assumption that the electrostatic potential is well described using such local or semilocal functionals. A hybrid functional study of Si and TiO_2 surfaces [12] and a self-consistent GW study of an Si/SiO_2 interface [13] have indeed shown that the changes in the averaged electrostatic potential from the semilocal values are less than 0.1 eV at these surfaces and interface. Another theoretical study using an approximate exact-exchange optimized effective potential suggests that the asymptotic behavior of an exchange-correlation potential at surfaces affects the electrostatic potential by up to ∼0.3 eV to lower the VBM or increase the IP [14]. Compared with the changes in these surface contributions, the shifts in the bulk band positions by hybrid functionals or GW are much larger and therefore dominantly contribute to the improvement in the predicted surface and interface band positions.

Previous studies indicate that hybrid functionals such as the forms of Perdew-Burke-Ernzerhof (PBE0) [15–17],

*yuuukuma@gmail.com
†oba@msl.titech.ac.jp

Heyd-Scuseria-Ernzerhof (HSE06) [18–20], and B3LYP [21], as well as screened exchange functionals [22], improve the band structures of semiconductors and insulators over local and semilocal functionals [20,23–27]. This is also the case with the band positions at surfaces [28] and heterointerfaces [29,30], but sizable differences from experimental values are still observed for the surface band positions of some systems such as sulfides and oxides [28]. The GW approximation [31] based on many-body perturbation theory does not necessarily perform better in the prediction of band alignment if a standard approach using the random-phase approximation for W is employed [12,28,30]. Vertex corrections in the self-energy lead to good agreement with experimental IP and EA values for a variety of surfaces [28,30], but such calculations are demanding. A computationally concise but sufficiently accurate approach is needed for a systematic evaluation of band structures and alignments, especially for high-throughput screening of candidate materials including as-yet-unreported ones [32–37].

The performance of hybrid functionals can be improved by tuning the amount of the nonlocal Fock exchange because the optimal nonlocal exchange mixing is system dependent, reflecting the strength of electronic screening [15,38,39]. It is fixed at one quarter in the HSE06 and PBE0 functionals on the basis of the connection with Møller-Plesset perturbation theory [15]. Some other hybrid functionals such as B3LYP also employ similar amounts of nonlocal exchange mixing, which are empirically determined to reproduce experimental physical quantities such as atomization energies. As a result, hybrid functionals tend to perform worse as electronic structures deviate more from those assumed in the construction of the functionals. For instance, the band gaps of wide-gap insulators such as MgO and NaCl are severely underestimated using HSE06 and PBE0 [27,40,41]. HSE06 well describes narrow or middle-sized gap semiconductors, as long as their electronic structures are not strongly localized [20]. PBE0 overestimates the gaps of narrow-gap semiconductors but performs better than HSE06 for wide-gap semiconductors and insulators such as ZnO and MgO [27,39,41,42]. Clearly, a system-dependent treatment of the nonlocal exchange mixing is required for simultaneously describing diverse materials. An empirical tuning of the mixing has been made to reproduce experimental band gaps and density of states, and/or other parameters [29,39,40,43], but this approach is inapplicable to materials for which experimental values are unavailable.

It has been discussed that the nonlocal exchange mixing in hybrid functionals can be related to the reciprocal of static dielectric constants on the basis of the static Coulomb hole plus screened exchange approximation to the electron self-energy [31,38,39]. Such parameterized functionals, denoted as dielectric-dependent hybrid functionals, have been reported to generally improve band gaps over standard HSE06 and PBE0 functionals [38,41,44–46]. This approach does not require the empirical parameter tuning. In addition, it is computationally less expensive than GW, especially if combined with a non-self-consistent treatment as reported by Tran [27]. Thus, the dielectric-dependent hybrid functionals would be suited for the prediction of surface and interface band positions as well as bulk band structures, but their performance in the band alignment has not been examined systematically for inorganic materials.

In the present study the band alignment of semiconductors and insulators is investigated using dielectric-dependent hybrid functionals. Prototypical systems in the diamond, zinc-blende, rocksalt, and wurtzite structures are considered for discussing their performance comparatively with the HSE06 hybrid functional. The effect of self-consistency on the prediction of the band structures and alignments is also discussed.

II. METHODS

A. Dielectric-dependent hybrid functionals

In the formalism of the generalized Kohn-Sham scheme [47], the nonlocal exchange-correlation potential of a full-range hybrid functional is given as

$$v_{\mathrm{xc}}(\mathbf{r},\mathbf{r}') = a v_{\mathrm{x}}^{\mathrm{nl}}(\mathbf{r},\mathbf{r}') + (1-a) v_{\mathrm{x}}^{\mathrm{l}}(\mathbf{r}) + v_{\mathrm{c}}(\mathbf{r}), \qquad (1)$$

where $v_{\mathrm{x}}^{\mathrm{nl}}(\mathbf{r},\mathbf{r}')$ and $v_{\mathrm{x}}^{\mathrm{l}}(\mathbf{r})$ denote nonlocal and (semi)local exchange potentials, respectively, and $v_{\mathrm{c}}(\mathbf{r})$ is a correlation potential. In PBE0, the nonlocal exchange mixing parameter a is set at one quarter, and the exchange and correlation potentials of the Perdew-Burke-Ernzerhof semilocal functional (PBE) [48] are used for $v_{\mathrm{x}}^{\mathrm{l}}(\mathbf{r})$ and $v_{\mathrm{c}}(\mathbf{r})$ [15–17]. HSE06 divides the exchange potential into short-range and long-range terms, where one quarter of nonlocal exchange is mixed only in the former and the exchange-correlation potential is otherwise treated using PBE [18–20].

By comparing Eq. (1) with the electron self-energy in the static Coulomb hole plus screened exchange approximation [31], the nonlocal exchange mixing parameter in the full-range hybrid functional is given as $a = \varepsilon_{\infty}^{-1}$, where ε_{∞} is the electronic contribution to the static dielectric constant of the system considered [38,44]. Equation (1) with $a = \varepsilon_{\infty}^{-1}$ thus constitutes a full-range dielectric-dependent hybrid functional. Range-separated dielectric-dependent hybrid functionals have also been proposed [45,46], with a slightly improved performance over full-range functionals [46]. We use the full-range form in the present study.

In principle, the nonlocal exchange mixing in the dielectric-dependent hybrid functional can be determined self-consistently so that the mixing value becomes consistent with the dielectric constant evaluated using that functional [44]. However, the use of dielectric constants from PBE or PBE0 calculations has previously been shown to provide reasonably good performance in the evaluation of band gaps while reducing computational costs [44]. We take this approach in the present study as we aim at establishing a computationally concise approach to the prediction of band structures and alignments.

Furthermore, non-self-consistent hybrid functional calculations can be effectively used when the self-consistency does not change wave functions significantly from the starting ones [27]. In the present study the eigenvalues were obtained by diagonalizing the Hamiltonian matrix once, where the matrix elements were constructed using PBE wave functions and charge density. This non-self-consistent scheme is different from the one reported by Tran, where only the diagonal terms of the Hamiltonian matrix are considered [27]. The

non-self-consistent approach significantly speeds up hybrid functional calculations by a factor of ∼10. It is especially advantageous in the evaluation of band alignments; the bulk eigenvalues can be exactly aligned with those of surfaces and interfaces treated using PBE because the electrostatic potential remains unchanged from that of PBE. The band positions at the surfaces and interfaces can thus be determined at the level of the non-self-consistent hybrid functional approach without expensive hybrid functional calculations of surfaces and interfaces. In combination with the automated generation of surface and interface simulation models (e.g., Ref. [49]), non-self-consistent hybrid functional calculations would allow us to do systematic study or high-throughput screening based on the band alignment.

B. Computational details

The calculations were performed using the projector augmented-wave (PAW) method [50] as implemented in the VASP code [51–53]. The full-range dielectric-dependent hybrid functional as well as the HSE06 and PBE0 hybrid functionals and the PBE semilocal functional were used depending on the objectives, as described later; in many cases, the hybrid functionals were applied non-self-consistently. The effect of spin-orbit coupling, which was previously evaluated using HSE06 [28], was considered as a correction to the band gap and the VBM (or IP) in all the results presented in this paper. A plane-wave cutoff energy of 550 eV was used in the calculations.

Prototypical systems that are crystallized in simple structures and well studied experimentally and/or theoretically are considered: C and Si in the diamond structure; BN, AlP, AlAs, AlSb, GaP, GaAs, InP, ZnS, ZnSe, ZnTe, CdS, CdSe, and CdTe in the zinc-blende structure; MgO in the rocksalt structure; and GaN and ZnO in the wurtzite structure. This excludes materials for which PBE gives no or rather narrow band gaps to avoid inaccurate band structures by non-self-consistent hybrid functional calculations on top of PBE or inaccurate dielectric constants obtained as described below using PBE. Experimental lattice parameters summarized in Ref. [28] were used to directly compare the theoretical band gaps, IPs, and EAs with experimental values. In the bulk calculations k-point meshes of $6 \times 6 \times 6$ for diamond, zinc-blende, and rocksalt crystals and $6 \times 6 \times 4$ for wurtzite crystals were employed.

To determine the nonlocal exchange mixing in the dielectric-dependent hybrid functional, the electronic contributions of the static dielectric constants were evaluated on the basis of density functional perturbation theory (DFPT) [54,55], using PBE with the random-phase approximation or local-field effects. A finite-electric-field approach [56] was also employed in combination with PBE0, which includes local-field effects. The number of k-point meshes in these calculations was increased at least by more than 2 times in all the directions from the aforementioned mesh so as to attain the convergence of dielectric constants within 0.2 with respect to the multiplication of the aforementioned k mesh. When PBE gives quite narrow band gaps, this convergence criterion requires a finer k mesh by up to 4 times in the DFPT calculations, while the PBE0 dielectric constants from the finite-electric-field approach tend to converge faster. In addition, relatively shallow semicore Zn $3d$ states of Zn compounds are underbound and hybridized too much with valence anion p states when treated using PBE [28]. This is most serious in ZnO among the compounds considered in the present study [57]. The Zn $3d$ states were therefore corrected using the PBE+U approach when dielectric constants were evaluated, where Dudarev's formulation [58] was used with $U_{\text{effective}}(=U-J)=5$ eV.

Nonpolar surfaces and interfaces were modeled using supercells with slab and superlattice geometries, respectively. The considered surfaces are (111) 2×1 for C and Si in the diamond structure, (110) for the zinc-blende crystals, (100) for MgO in the rocksalt structure, and $(11\bar{2}0)$ for GaN and ZnO in the wurtzite structure. The (110) surfaces of the zinc-blende crystals were treated using 14-layer-thick slabs separated by a vacuum region with the same thickness, which amounts to 18–39 Å depending on the system. In these surface calculations $6 \times 4 \times 1$ k points were taken. Similar slab and vacuum thicknesses and k-point densities were used for the other surfaces. The in-plane lattice parameters were fixed to the PBE-optimized bulk values, and the internal coordinates were relaxed using PBE. Subsequently, PBE calculations were conducted without further atomic relaxation after scaling the lattice constants to the experimental values. The IPs and EAs were then evaluated in conjunction with bulk results, respectively, as

$$I = \epsilon_{\text{vac-ref}} - \epsilon_{\text{VBM-ref}} \tag{2}$$

and

$$A = \epsilon_{\text{vac-ref}} - \epsilon_{\text{CBM-ref}}, \tag{3}$$

where $\epsilon_{\text{vac-ref}}$ is the energy difference between the vacuum level and the electrostatic reference level in a bulklike region of a surface supercell. The reference level was determined by averaging the local Kohn-Sham potential within PAW spheres over atomic sites located in a region far from the surface within a thickness of one third of the slab. $\epsilon_{\text{VBM-ref}}$ ($\epsilon_{\text{CBM-ref}}$) is the energy difference between the VBM (CBM) and the electrostatic reference level from bulk calculations. This contribution was evaluated using PBE or non-self-consistent hybrid functional calculations on top of PBE. In previous studies, macroscopically averaged electrostatic potential in the bulk region has been widely used as the electrostatic reference level [10,59]. The typical change in the IPs and EAs is less than 0.03 eV and at most 0.09 eV for the 18 systems considered here when this approach is taken. The macroscopically averaged electrostatic potential is also used in the present study to discuss the effects of self-consistency in Sec. III A.

Nonpolar (110) heterointerfaces between selected zinc-blende crystals were considered using supercells with 11 layers for each crystal and $6 \times 4 \times 1$ k points. The in-plane lattice parameters were fixed to the average of the PBE lattice parameters of the two constituent crystals, and the out-of-plane lattice parameter and internal coordinates were relaxed using PBE. Natural (unstrained) interfacial band offsets at experimental lattice constants were obtained using a procedure reported in Ref. [60], where the results for the strained interface, strained and unstrained surfaces, and unstrained bulk systems were combined. More details of the surface and interface calculations and the derivation of IPs, EAs, and interfacial band offsets have been reported in Refs. [30,60,61].

III. RESULTS AND DISCUSSION

A. Effects of self-consistency

The effects of self-consistency are investigated using the results of self-consistent and non-self-consistent HSE06 calculations for the identical bulk and surface cells. As shown in Fig. 1, the differences in the band gap between the self-consistent and non-self-consistent cases are overall small, ∼0.1 eV or less. Figure 2 compares the band structures of Si and ZnO obtained using self-consistent and non-self-consistent HSE06 calculations. The self-consistent and non-self-consistent results are almost identical for Si. In the case of ZnO, the Zn 3*d* states located around −6 eV are slightly deeper in the non-self-consistent result. The band structure is otherwise similar. The non-self-consistent approach appears to work well for the systems considered here; however, it should be carefully used in cases where band inversion occurs at self-consistent steps from PBE to hybrids.

As in the case of the band gaps, the self-consistency does not significantly affect the VBM and CBM with respect to the vacuum level, i.e., the negatives of the IP and EA, respectively. The differences between the self-consistent and non-self-consistent values are typically ∼0.1 eV. Exceptions are MgO and ZnO, which exhibit ∼0.4 eV differences, and GaN, with an ∼0.2 eV difference. Figure 1 also shows the differences in the slab electrostatic potential between self-consistent and non-self-consistent cases: the former and the latter have been determined at the HSE06 and PBE levels, respectively. The results imply that the differences between the self-consistent and non-self-consistent IP values for MgO and GaN are mostly attributed to the differences in the slab electrostatic potential originating from the changes in surface dipoles. In ZnO, about half the difference appears to come from this contribution. The charge density, and therefore electrostatic potential, is reconstructed relatively largely at the self-consistent steps in these systems. This can be recognized in Fig. 3, where the differences in the charge density between the self-consistent and non-self-consistent results are visualized for the BN, MgO, and ZnO surfaces. In the case of BN almost no difference is found, while discrepancies are noticeable at the O sites in MgO and both Zn and O sites in ZnO. Relatively large changes by self-consistency in these oxides can be attributed to the large changes in the band structures, in particular band gaps, which affect the orbital hybridization and thereby the charge transfer from cations to anions. In addition, the Zn 3*d* and O 2*p* states are energetically close in the valence band of ZnO, and the degree of their hybridization changes with self-consistency, as also recognized in the band structures shown in Fig. 2. These changes in the charge density prevail throughout the slabs including bulk regions. Such a change in the bulk charge density necessarily changes the surface charge density and therefore surface dipoles [63]. This effect is likely to be dominant in MgO and ZnO since the degree of the charge density reconstruction at these surfaces is similar to the respective bulk regions; ZnO shows an anisotropic distribution of the charge density difference around the surface O sites, which should also contribute to the change in the surface dipole.

In a previous study ∼0.4 eV differences have been found in the IPs of MgO and ZnO between GW_0 on top of PBE and $GW^{\mathrm{TC-TC}}$ on top of HSE06, while the results for other compound semiconductors are similar between the two approaches [28]. This would also be explained by the different treatment of the Hartree potential, using either PBE or HSE06.

In summary, the self-consistency affects band gaps by only ∼0.1 eV for all materials considered here, while affecting the IP and EA by ∼0.4 eV for MgO and ZnO, ∼0.2 eV for GaN, and ∼0.1 eV for the others. This margin of error should be considered in the discussion on the band alignment.

B. Dielectric constants and band gaps

The dielectric constants are discussed here as they play essential roles in the dielectric-dependent hybrid functional. The calculated static electronic dielectric constants are listed in Table I. The PBE0 dielectric constants are generally close to the experimental values. Following a previous study by Skone *et al.* [44], local-field effects are included in the evaluation: the dielectric constants are generally underestimated without local-field effects, leading to the overestimation of band gaps by the dielectric-dependent hybrid functional. The dielectric constants calculated using PBE(+U) tend to be overestimated, mainly because of the band gap underestimation. PBE(+U) with the random-phase approximation (RPA) yields smaller values than that with local-field effects, and the resultant dielectric constants are closer to the PBE0 and experimental

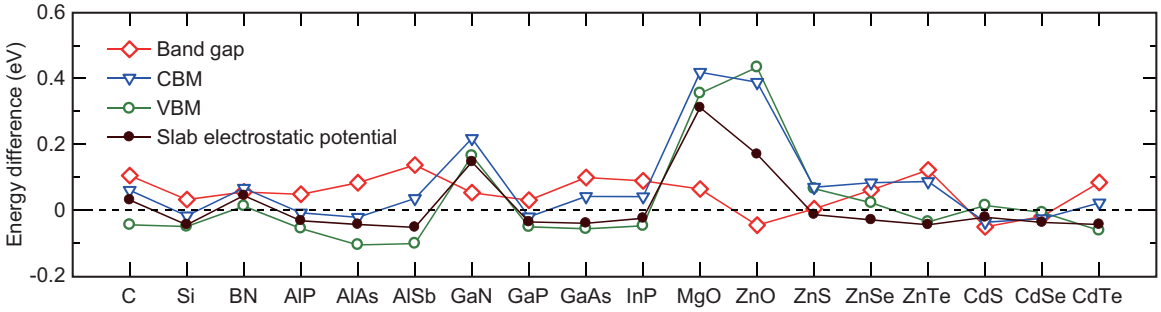

FIG. 1. Differences in the band gap, CBM, VBM, and macroscopically averaged slab electrostatic potential between self-consistent and non-self-consistent HSE06 calculations using the identical bulk and surface cells. The plotted energy differences correspond to the values from the self-consistent calculations with respect to those from the non-self-consistent calculations. The CBM, VBM, and slab electrostatic potential are measured with respect to the vacuum level. Note that the electrostatic potential is determined using HSE06 in the self-consistent approach while it is treated at the PBE level in the non-self-consistent case.

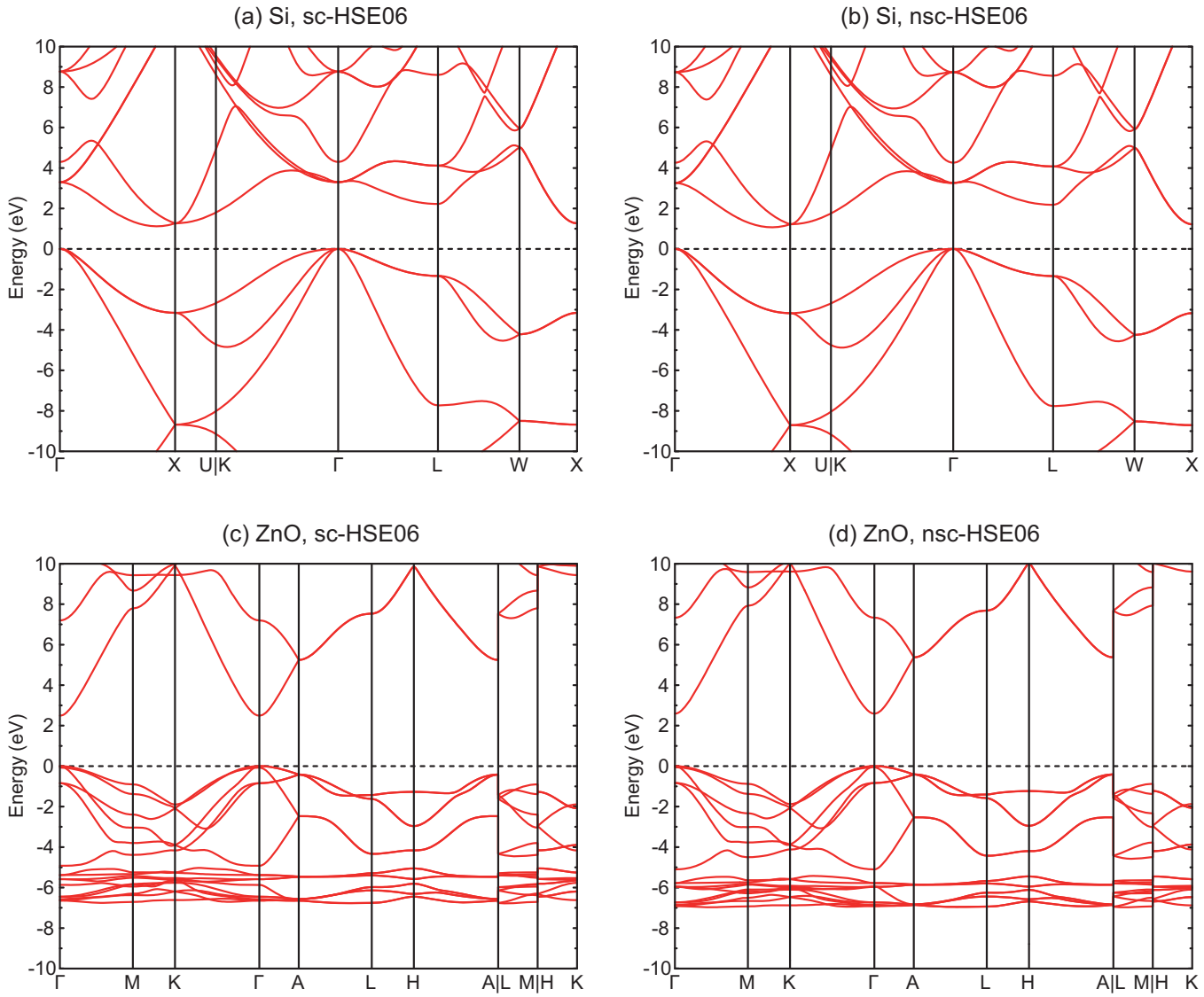

FIG. 2. Band structures of (a) and (b) Si and (c) and (d) ZnO obtained using self-consistent (sc) and non-self-consistent (nsc) HSE06 calculations. The origin of the energy is set at the valence band maximum. Band paths reported in Ref. [62] are used.

values. This fortuitous tendency can explain the success of GW calculations using W from PBE($+U$) with the RPA, which yield similar results to those using vertex-corrected, self-consistently determined W [65].

In the present study we consider the dielectric constants obtained using PBE($+U$) with the RPA in addition to PBE0 with local-field effects. The former requires much lower computational costs but performs reasonably well in the prediction of band gaps and alignments, as shown below.

Table II and Fig. 4 show band gaps obtained using various approximations. PBE significantly underestimates the band gaps of all systems, which is a tendency well recognized. The HSE06 hybrid functional improves the band gap prediction. Still, underestimation is obvious for BN, ZnO, and MgO with wide band gaps; here the non-self-consistent approach is taken, but self-consistency does not significantly affect the band gaps, as discussed in Sec. III A. The dielectric-dependent hybrid functionals, which are also used non-self-consistently, yield band gaps closer to the experimental values than HSE06 for such wide-gap systems; the band gaps are not significantly affected by the choice of the dielectric constants, the values using PBE($+U$) with the RPA, or PBE0 with local-field effects. On the other hand, the performance of the dielectric-dependent hybrid functionals is comparable with HSE06 for narrow-gap systems. An exception is GaAs, for which the underestimation of the band gap is more enhanced with the dielectric-dependent hybrid functionals. These overall tendencies are consistent with previous reports by Marques *et al.* [38], Skone *et al.* [44], and Gerosa *et al.* [41].

C. Band alignment at surfaces

Figure 5 shows the VBM and CBM with respect to the vacuum level, which are negatives of the IP and EA, respectively. Our previous GW_0@PBE results [28] are also included for comparison, which are based on the same PBE calculations as in the present study; the VBM and CBM predicted by GW are much improved with self-energy vertex corrections, but such results are so far available for only those

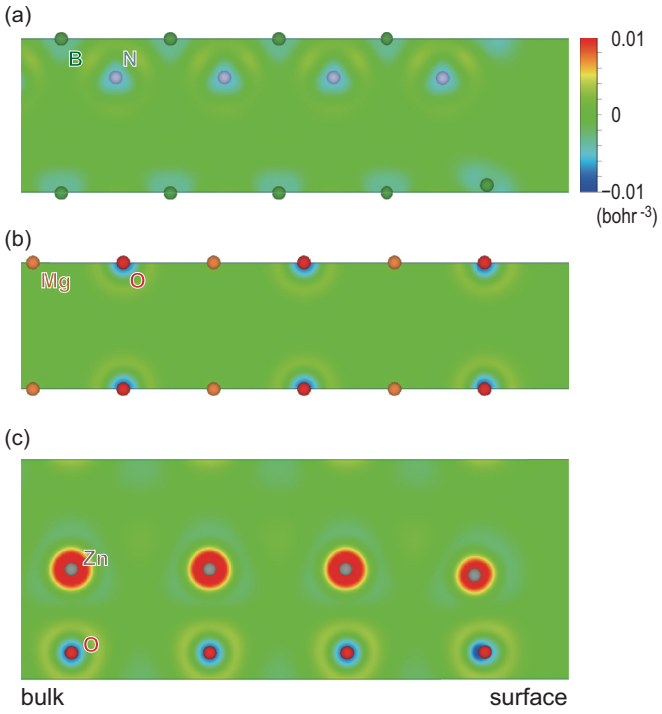

FIG. 3. Differences in the charge density of surface slab models between self-consistent and non-self-consistent HSE06 calculations for (a) BN, (b) MgO, and (c) ZnO. The values from the self-consistent calculations with respect to those from the non-self-consistent calculations are plotted on planes perpendicular to the surfaces. Note that the charge density is determined using HSE06 in the self-consistent approach while it is treated at the PBE level in the non-self-consistent case.

obtained on top of HSE06 [28,30]. The experimental VBM or IP reported for the nonpolar surfaces that have orientations and reconstructed structures identical to those considered in our calculations are also shown [66,67]; an exception is GaN, for which experimental band positions for polar {0001} surfaces are instead presented because values for nonpolar surfaces are not available. The experimental CBM is estimated by adding an experimental band gap to the VBM, where the experimental values listed in Table II are used.

The experimental values show a spread, in particular for C and CdS. This is partly due to the sensitivity of the band positions to the characters of surfaces, not only orientations and reconstructed structures but also chemistry and adsorption. This makes a direct comparison between experiment and theory difficult in some cases. Nevertheless, it is clear that PBE yields systematically too high VBM with respect to the vacuum level or too small IP. The VBM of most systems is slightly too high with the hybrid functionals, while the GW_0@PBE values are too low at a similar magnitude. In this sense, the hybrid functionals can predict the VBM positions almost on par with GW_0@PBE. Among the hybrid functionals, noticeable differences are found for MgO and ZnO. Non-self-consistent HSE06 tends to yield a VBM higher than the experimental value, while the values with dielectric-dependent hybrid functionals are lower. As discussed in Sec. III A, the self-consistent HSE06 calculations show ∼0.4 eV higher

TABLE I. Static electronic dielectric constants obtained using PBE(+U) with the random-phase approximation ($\varepsilon_\infty^{\mathrm{PBE-RPA}}$), PBE(+$U$) with local-field effects ($\varepsilon_\infty^{\mathrm{PBE}}$), and PBE0 with local-field effects ($\varepsilon_\infty^{\mathrm{PBE0}}$). Experimental values summarized in Ref. [64] are also shown. Mean absolute errors (MAEs) with respect to the experimental values are listed in the bottom row.

	$\varepsilon_\infty^{\mathrm{PBE-RPA}}$	$\varepsilon_\infty^{\mathrm{PBE}}$	$\varepsilon_\infty^{\mathrm{PBE0}}$	Experiment
C	5.5	5.9	5.4	5.7
Si	12.1	12.9	10.9	11.6
BN	4.4	4.6	4.4	4.46
AlP	7.5	8.1	7.1	7.4
AlAs	8.6	9.3	8.0	8.16
AlSb	10.7	11.5	9.8	9.88
GaN	5.5	5.8	5.0	5.4
GaP	9.7	10.4	8.7	8.8
GaAs	12.9	13.7	10.1	10.86
InP	10.3	11.0	8.7	9.9
MgO	3.0	3.1	2.9	3.1
ZnO	4.8	5.0	3.6	3.7
ZnS	5.6	5.9	5.1	5.1
ZnSe	6.7	7.2	5.9	5.9
ZnTe	8.3	8.9	7.2	6.9
CdS	5.7	6.1	5.1	5.4
CdSe	7.2	7.6	5.9	6.2
CdTe	8.1	8.6	6.9	7.1
MAE	0.7	1.1	0.3	

VBMs than the non-self-consistent results for MgO and ZnO, deviating more from the experimental values. Assuming the same tendency with dielectric-dependent hybrid functionals, the agreement with experiment would become much better than HSE06 when treated self-consistently.

Turning to the CBM, PBE shows good agreement with experiment, except for GaN, MgO, and ZnO, for which the CBMs are too deep with respect to the vacuum level. The hybrid functionals improve the CBM of these materials. It appears that the CBMs from the hybrid functionals are better than GW_0@PBE. Among the hybrid functionals considered, the dielectric-dependent hybrid functionals yield better agreement with experiment than HSE06 for MgO and ZnO. This is partly due to the improvement in the band gap prediction; as shown in Sec. III B, non-self-consistent HSE06 calculations underestimate the band gaps of MgO and ZnO by 1.3 and 0.8 eV, respectively, while the dielectric-dependent hybrid functionals reproduce the band gap with errors of 0.3 and 0.1 eV. This superior feature of the dielectric-dependent hybrid functionals would, however, be weakened with self-consistency, where the CBMs of MgO and ZnO are raised by ∼0.4 eV in the case of the HSE06 results shown in Fig. 1.

Overall, the performance of the non-self-consistent hybrid functionals, particularly dielectric-dependent ones, is remarkable. It is also noted that they are more advantageous than GW in terms of computational costs, especially when PBE-RPA dielectric constants are used.

D. Band alignment at heterointerfaces

The calculated natural valence band offsets at zinc-blende (110) heterointerfaces are listed in Table III, along with

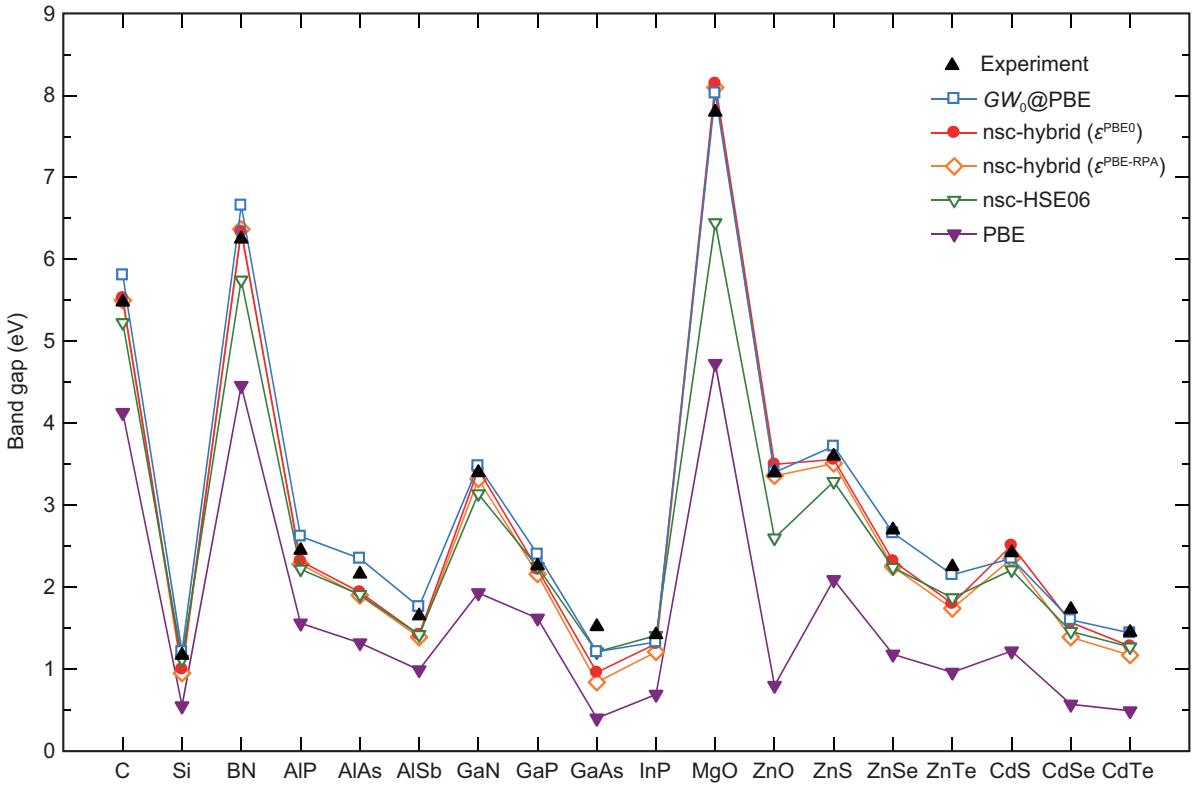

FIG. 4. Band gaps obtained using various approximations compared with reported GW_0@PBE and experimental values. Here nsc-hybrid($\varepsilon_\infty^{\mathrm{PBE-RPA}}$) and nsc-hybrid($\varepsilon_\infty^{\mathrm{PBE0}}$) denote non-self-consistent dielectric-dependent hybrid functionals with static electronic dielectric constants obtained using PBE($+U$) with the RPA and PBE0 with local-field effects, respectively. The GW_0@PBE and experimental values are taken from Ref. [28].

TABLE II. Band gaps obtained using various approximations compared with reported GW_0@PBE and experimental values (in eV). Here nsc-hybrid($\varepsilon_\infty^{\mathrm{PBE-RPA}}$) and nsc-hybrid($\varepsilon_\infty^{\mathrm{PBE0}}$) denote non-self-consistent dielectric-dependent hybrid functionals with static electronic dielectric constants obtained using PBE($+U$) with the RPA and PBE0 with local-field effects, respectively. The GW_0@PBE and experimental values are taken from Ref. [28]. Mean absolute errors (MAEs) with respect to the experimental values are listed in the bottom row.

	PBE	nsc-HSE06	nsc-hybrid($\varepsilon_\infty^{\mathrm{PBE-RPA}}$)	nsc-hybrid($\varepsilon_\infty^{\mathrm{PBE0}}$)	GW_0@PBE	Experiment
C	4.13	5.23	5.50	5.53	5.81	5.48
Si	0.55	1.12	0.95	1.01	1.21	1.17
BN	4.46	5.75	6.37	6.34	6.66	6.25
AlP	1.56	2.22	2.28	2.32	2.62	2.45
AlAs	1.32	1.91	1.90	1.94	2.35	2.16
AlSb	0.99	1.42	1.39	1.42	1.76	1.65
GaN	1.93	3.14	3.32	3.44	3.48	3.4
GaP	1.62	2.25	2.16	2.22	2.40	2.26
GaAs	0.40	1.21	0.84	0.96	1.21	1.52
InP	0.69	1.41	1.21	1.31	1.33	1.42
MgO	4.73	6.45	8.10	8.15	8.03	7.8
ZnO	0.80	2.60	3.36	3.50	3.40	3.4
ZnS	2.09	3.29	3.51	3.56	3.72	3.6
ZnSe	1.18	2.24	2.25	2.32	2.66	2.7
ZnTe	0.96	1.87	1.74	1.80	2.15	2.25
CdS	1.22	2.21	2.35	2.51	2.35	2.42
CdSe	0.57	1.46	1.39	1.57	1.60	1.73
CdTe	0.49	1.27	1.17	1.28	1.44	1.45
MAE	1.30	0.34	0.23	0.19	0.14	

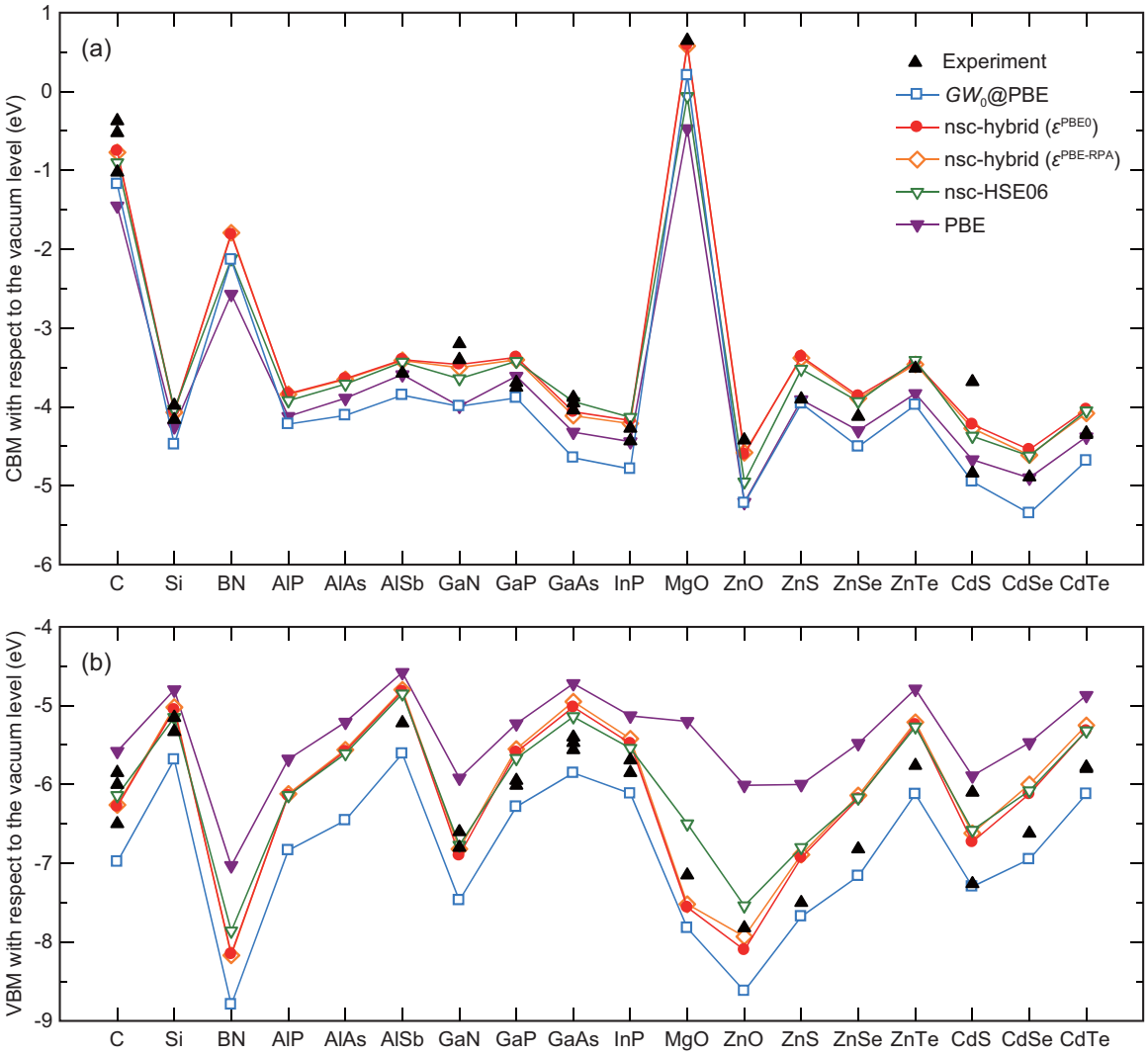

FIG. 5. (a) CBM and (b) VBM with respect to the vacuum level (negatives of the EA and IP, respectively) obtained using various approximations compared with reported GW_0@PBE and experimental values. Here nsc-hybrid($\varepsilon_\infty^{\mathrm{PBE-RPA}}$) and nsc-hybrid($\varepsilon_\infty^{\mathrm{PBE0}}$) denote non-self-consistent dielectric-dependent hybrid functionals with static electronic dielectric constants obtained using PBE($+U$) with the RPA and PBE0 with local-field effects, respectively. The GW_0@PBE values are taken from Ref. [28]. The experimental values are for the nonpolar surfaces identical to those considered in the present study [66,67]; an exception is GaN, for which experimental values for polar {0001} surfaces are shown. The experimental CBM is estimated by adding a reported experimental band gap to the VBM (see Table II).

TABLE III. Natural valence band offsets at zinc-blende (110) heterointerfaces obtained using various approximations compared with reported GW_0@PBE and experimental values (in eV). Positive values mean that the valence band maximum of semiconductor A is higher than that of semiconductor B at the A/B heterointerface. Here nsc-hybrid($\varepsilon_\infty^{\mathrm{PBE-RPA}}$) and nsc-hybrid($\varepsilon_\infty^{\mathrm{PBE0}}$) denote non-self-consistent dielectric-dependent hybrid functionals with static electronic dielectric constants obtained using PBE($+U$) with the RPA and PBE0 with local-field effects, respectively. The GW_0@PBE values are taken from Ref. [30], while the experimental values are from Refs. [68–75]. Note that the experimental values are not necessarily for the (110) heterointerfaces.

Interface (A/B)	PBE	nsc-HSE06	nsc-hybrid($\varepsilon_\infty^{\mathrm{PBE-RPA}}$)	nsc-hybrid($\varepsilon_\infty^{\mathrm{PBE0}}$)	GW_0@PBE	Experiment
GaP/AlP	0.46	0.48	0.58	0.56	0.56	0.57 [68], 0.43 [69]
GaAs/AlAs	0.45	0.43	0.57	0.52	0.56	0.40 [70], 0.15 [70], 0.55 [71]
GaAs/ZnSe	0.65	0.92	1.08	1.06	1.20	0.96 [72], 1.10 [72]
AlSb/ZnTe	0.24	0.46	0.44	0.45	0.55	0.42 ± 0.07 [73], 0.35 ± 0.11 [74]
ZnTe/CdSe	0.62	0.75	0.74	0.82	0.77	0.64 ± 0.07 [75]

experimental values. Interfaces with small lattice misfits between the constituent crystals (less than 0.5%) are selected to reduce the ambiguity associated with possible strain effects. The experimental values listed in Table III are not necessarily for the (110) heterointerfaces considered in the present calculations. In addition, atomically flat interfaces without interdiffusion have been modeled in the present study, while actual interfaces may include misfit dislocations to relieve the strain [76–78], reconstruction at the atomic level, and/or interdiffusion [79]. Still, a comparison between theory and experiment would be meaningful, assuming that these effects on interfacial band offsets are not significant at the considered interfaces composed of the isostructural crystals with small lattice mismatches.

Compared with the surface band positions, the dependence on the approximation is smaller due to the cancellation effects between the two interface constituents. Therefore, even PBE gives reasonable values with some exceptions. Although the experimental values are not necessarily for the (110) interfaces and show a spread, the hybrid functionals appear to yield values closer to experiment. Again, their performance is almost on par with $G W_0$@PBE. For the interface constituents considered here, the differences between the non-self-consistent HSE06 and dielectric-dependent hybrid functionals are small for both band gaps and surface VBM positions. As a result, similar values are obtained for the valence band offsets. The situation would, however, be different when wide-gap oxides such as MgO and ZnO are involved, for which improved band gaps by dielectric-dependent hybrid functionals are expected to provide better predictions of the valence and/or conduction band offsets.

IV. CONCLUSIONS

The band gaps, surface band positions, and interfacial band offsets of 18 prototypical semiconductors and insulators have been investigated using hybrid functionals. The self-consistent and non-self-consistent HSE06 calculations yield band gaps close to each other for all the systems considered: the differences are only ∼0.1 eV. Surface band positions also agree at a similar level, except for ZnO and MgO, with ∼0.4 eV differences, and GaN, with an ∼0.2 eV difference. Apart from these discrepancies, the non-self-consistent approach is advantageous as it can greatly reduce computational costs.

The performance of dielectric-dependent hybrid functionals, where the nonlocal Fock exchange mixing is set at the reciprocal of static electronic dielectric constants, has been investigated for predicting band gaps and alignments. Improvements over the HSE06 hybrid functional are found for the band gaps and surface band alignments of wide-gap systems. The band offsets at selected heterointerfaces are predicted with a similar degree of precision. The present study focuses on prototypical semiconductors and insulators that have relatively simple band structures for benchmarking purposes, while previous dielectric-dependent hybrid functional studies have demonstrated good descriptions of electronically more complex systems such as 3*d* transition-metal oxides as well [27,41,44]. Thus, the dielectric-dependent hybrid functional in conjunction with the non-self-consistent treatment is suited for high-throughput calculations that require both efficiency and accuracy.

ACKNOWLEDGMENTS

This work was supported by the MEXT Elements Strategy Initiative to Form Core Research Center, Grants-in-Aid for Scientific Research B (Grant No. 15H04125) and Scientific Research on Innovative Areas (Grant No. 25106005) from JSPS, and PRESTO and the Support Program for Starting Up Innovation Hub MI^{2}I from JST, Japan. Computing resources of ACCMS at Kyoto University were used.

[1] E. T. Yu, J. O. McCaldin, and T. C. McGill, *Solid State Physics* (Academic, Boston, 1992), p. 1.
[2] A. Franciosi and C. G. Van de Walle, Surf. Sci. Rep. **25**, 1 (1996).
[3] D. Cahen and A. Kahn, Adv. Mater. **15**, 271 (2003).
[4] J. Robertson, J. Vac. Sci. Technol. A **31**, 050821 (2013).
[5] H. Hosono, *Transparent Electronics: From Synthesis to Applications* (Wiley, Hoboken, NJ, 2010), Chap. 2, p. 34.
[6] K. Hashimoto, H. Irie, and A. Fujishima, Jpn. J. Appl. Phys. **44**, 8269 (2005).
[7] S. J. A. Moniz, S. A. Shevlin, D. J. Martin, Z.-X. Guo, and J. Tang, Energy Environ. Sci. **8**, 731 (2015).
[8] Y. Ping, D. Rocca, and G. Galli, Chem. Soc. Rev. **42**, 2437 (2013).
[9] M. S. Hybertsen and S. G. Louie, Phys. Rev. B **34**, 5390 (1986).
[10] K. Steiner, W. Chen, and A. Pasquarello, Phys. Rev. B **89**, 205309 (2014).
[11] V. Stevanović, S. Lany, D. S. Ginley, W. Tumas, and A. Zunger, Phys. Chem. Chem. Phys. **16**, 3706 (2014).
[12] W. Chen and A. Pasquarello, Phys. Rev. B **90**, 165133 (2014).
[13] R. Shaltaf, G.-M. Rignanese, X. Gonze, F. Giustino, and A. Pasquarello, Phys. Rev. Lett. **100**, 186401 (2008).
[14] L.-H. Ye, Phys. Rev. B **94**, 035113 (2016).
[15] J. P. Perdew, M. Ernzerhof, and K. Burke, J. Chem. Phys. **105**, 9982 (1996).
[16] C. Adamo and V. Barone, J. Chem. Phys. **110**, 6158 (1999).
[17] M. Ernzerhof and G. E. Scuseria, J. Chem. Phys. **110**, 5029 (1999).
[18] J. Heyd, G. E. Scuseria, and M. Ernzerhof, J. Chem. Phys. **118**, 8207 (2003).
[19] J. Heyd, G. E. Scuseria, and M. Ernzerhof, J. Chem. Phys. **124**, 219906 (2006).
[20] A. V. Krukau, O. A. Vydrov, A. F. Izmaylov, and G. E. Scuseria, J. Chem. Phys. **125**, 224106 (2006).
[21] A. D. Becke, J. Chem. Phys. **98**, 5648 (1993).
[22] D. M. Bylander and L. Kleinman, Phys. Rev. B **41**, 7868 (1990).
[23] J. Paier, M. Marsman, K. Hummer, G. Kresse, I. C. Gerber, and J. G. Ángyán, J. Chem. Phys. **124**, 154709 (2006).
[24] R. Asahi, W. Mannstadt, and A. J. Freeman, Phys. Rev. B **59**, 7486 (1999).

[25] S. J. Clark and J. Robertson, Phys. Rev. B **82**, 085208 (2010).
[26] F. Oba, A. Togo, I. Tanaka, K. Watanabe, and T. Taniguchi, Phys. Rev. B **81**, 075125 (2010).
[27] F. Tran, Phys. Lett. A **376**, 879 (2012).
[28] A. Grüneis, G. Kresse, Y. Hinuma, and F. Oba, Phys. Rev. Lett. **112**, 096401 (2014).
[29] A. Alkauskas, P. Broqvist, F. Devynck, and A. Pasquarello, Phys. Rev. Lett. **101**, 106802 (2008).
[30] Y. Hinuma, A. Grüneis, G. Kresse, and F. Oba, Phys. Rev. B **90**, 155405 (2014).
[31] L. Hedin, Phys. Rev. **139**, A796 (1965).
[32] S. Curtarolo, G. L. W. Hart, M. B. Nardelli, N. Mingo, S. Sanvito, and O. Levy, Nat. Mater. **12**, 191 (2013).
[33] I. E. Castelli, T. Olsen, S. Datta, D. D. Landis, S. Dahl, K. S. Thygesen, and K. W. Jacobsen, Energy Environ. Sci. **5**, 5814 (2012).
[34] G. Hautier, A. Miglio, G. Ceder, G.-M. Rignanese, and X. Gonze, Nat. Commun. **4**, 2292 (2013).
[35] A. Zakutayev, A. J. Allen, X. Zhang, J. Vidal, Z. Cui, S. Lany, M. Yang, F. J. DiSalvo, and D. S. Ginley, Chem. Mater. **26**, 4970 (2014).
[36] R. Gautier, X. Zhang, L. Hu, L. Yu, Y. Lin, T. O. L. Sunde, D. Chon, K. R. Poeppelmeier, and A. Zunger, Nat. Chem. **7**, 308 (2015).
[37] Y. Hinuma, T. Hatakeyama, Y. Kumagai, L. A. Burton, H. Sato, Y. Muraba, S. Iimura, H. Hiramatsu, I. Tanaka, H. Hosono, and F. Oba, Nat. Commun. **7**, 11962 (2016).
[38] M. A. L. Marques, J. Vidal, M. J. T. Oliveira, L. Reining, and S. Botti, Phys. Rev. B **83**, 035119 (2011).
[39] A. Alkauskas, P. Broqvist, and A. Pasquarello, Phys. Status Solidi (b) **248**, 775 (2011).
[40] W. Chen, C. Tegenkamp, H. Pfnür, and T. Bredow, Phys. Rev. B **82**, 104106 (2010).
[41] M. Gerosa, C. E. Bottani, L. Caramella, G. Onida, C. Di Valentin, and G. Pacchioni, Phys. Rev. B **91**, 155201 (2015).
[42] F. Oba, M. Choi, A. Togo, and I. Tanaka, Sci. Technol. Adv. Mater. **12**, 034302 (2011).
[43] F. Oba, A. Togo, I. Tanaka, J. Paier, and G. Kresse, Phys. Rev. B **77**, 245202 (2008).
[44] J. H. Skone, M. Govoni, and G. Galli, Phys. Rev. B **89**, 195112 (2014).
[45] T. Shimazaki and T. Nakajima, J. Chem. Phys. **141**, 114109 (2014).
[46] J. H. Skone, M. Govoni, and G. Galli, Phys. Rev. B **93**, 235106 (2016).
[47] A. Seidl, A. Görling, P. Vogl, J. A. Majewski, and M. Levy, Phys. Rev. B **53**, 3764 (1996).
[48] J. P. Perdew, K. Burke, and M. Ernzerhof, Phys. Rev. Lett. **77**, 3865 (1996).
[49] Y. Hinuma, Y. Kumagai, F. Oba, and I. Tanaka, Comput. Mater. Sci. **113**, 221 (2016).
[50] P. E. Blöchl, Phys. Rev. B **50**, 17953 (1994).
[51] G. Kresse and J. Furthmüller, Phys. Rev. B **54**, 11169 (1996).
[52] G. Kresse and D. Joubert, Phys. Rev. B **59**, 1758 (1999).
[53] J. Paier, R. Hirschl, M. Marsman, and G. Kresse, J. Chem. Phys. **122**, 234102 (2005).
[54] S. Baroni and R. Resta, Phys. Rev. B **33**, 7017 (1986).
[55] M. Gajdoš, K. Hummer, G. Kresse, J. Furthmüller, and F. Bechstedt, Phys. Rev. B **73**, 045112 (2006).
[56] R. W. Nunes and X. Gonze, Phys. Rev. B **63**, 155107 (2001).
[57] F. Oba, M. Choi, A. Togo, A. Seko, and I. Tanaka, J. Phys. Condens. Matter **22**, 384211 (2010).
[58] S. L. Dudarev, G. A. Botton, S. Y. Savrasov, C. J. Humphreys, and A. P. Sutton, Phys. Rev. B **57**, 1505 (1998).
[59] C. G. Van de Walle and R. M. Martin, Phys. Rev. B **35**, 8154 (1987).
[60] Y. Hinuma, F. Oba, Y. Kumagai, and I. Tanaka, Phys. Rev. B **88**, 035305 (2013).
[61] Y. Hinuma, F. Oba, Y. Kumagai, and I. Tanaka, Phys. Rev. B **86**, 245433 (2012).
[62] Y. Hinuma, G. Pizzi, Y. Kumagai, F. Oba, and I. Tanaka, Comput. Mater. Sci. **128**, 140 (2017).
[63] Y. Kumagai, K. T. Butler, A. Walsh, and F. Oba (unpublished).
[64] S. Adachi, *The Handbook on Optical Constants of Semiconductors* (World Scientific, Singapore, 2012).
[65] M. Shishkin, M. Marsman, and G. Kresse, Phys. Rev. Lett. **99**, 246403 (2007).
[66] W. Mönch, *Semiconductor Surfaces and Interfaces* (Springer, Berlin, 2001).
[67] T. Jaouen, G. Jézéquel, G. Delhaye, B. Lépine, P. Turban, and P. Schieffer, Appl. Phys. Lett. **97**, 232104 (2010).
[68] S. Nagao, T. Fujimori, H. Gotoh, H. Fukushima, T. Takano, H. Ito, S. Koshihara, and F. Minami, J. Appl. Phys. **81**, 1417 (1997).
[69] J. R. Waldrop, R. W. Grant, and E. A. Kraut, J. Vac. Sci. Technol. B **11**, 1617 (1993).
[70] J. R. Waldrop, S. P. Kowalczyk, R. W. Grant, E. A. Kraut, and D. L. Miller, J. Vac. Sci. Technol. **19**, 573 (1981).
[71] J. Batey and S. L. Wright, J. Appl. Phys. **59**, 200 (1986).
[72] S. P. Kowalczyk, E. A. Kraut, J. R. Waldrop, and R. W. Grant, J. Vac. Sci. Technol. **21**, 482 (1982).
[73] E. T. Yu, M. C. Phillips, D. H. Chow, D. A. Collins, M. W. Wang, J. O. McCaldin, and T. C. McGill, Phys. Rev. B **46**, 13379 (1992).
[74] G. P. Schwartz, G. J. Gualtieri, R. D. Feldman, R. F. Austin, and R. G. Nuzzo, J. Vac. Sci. Technol. B **8**, 747 (1990).
[75] E. T. Yu, M. C. Phillips, J. O. McCaldin, and T. C. McGill, J. Vac. Sci. Technol. B **9**, 2233 (1991).
[76] J. W. Matthews and A. E. Blakeslee, J. Cryst. Growth **27**, 118 (1974).
[77] Y. Hinuma, F. Oba, and I. Tanaka, Phys. Rev. B **88**, 075319 (2013).
[78] J. G. Belk, J. L. Sudijono, X. M. Zhang, J. H. Neave, T. S. Jones, and B. A. Joyce, Phys. Rev. Lett. **78**, 475 (1997).
[79] F. Oba, F. Ernst, Y. Yu, R. Liu, H. M. Kothari, and J. A. Switzer, J. Am. Ceram. Soc. **88**, 253 (2005).